Faten B. Mohammed Ameen
Ghazwan G. Ali
Marwan H. Younus

Department of Physics, College of Education for Pure Sciences, Mosul University, Mosul, IRAQ

Fabrication and Characterization of Gas Sensors from ZnS/Porous Silicon Heterojunctions

ZnS-PSi heterojunction based gas sensor was fabricated in this study. ZnS thin film as the active materials over PSi substrate was synthesized by spray pyrolysis method. The effected of different concentration of ZnS (0.1M , 0.3 M and 0.5 M) on the characterization of the sensor have been investigated. The XRD results show that the ZnS has a hexagonal structure. SEM images were revealed that the ZnS as a circular grains with different sizes is synthesized over the PSi substrate. The electrical properties of the prepared sensor were proved that the sensitivity of the sensor is improved by increasing the concentration the ZnS. Furthermore, the ZnS-PSi heterojunction based gas sensor display high sensitivity and fast response and recovery times. The maximum sensitivity is found to be 5.11 when the ZnS concentration is 0.5 M compared to the sensitivity of 3.14 when the ZnS concentration is 0.1M. The ZnS-PSi heterojunction based gas sensor may be used for UV-light photo-detectors due to a valuable properties such as high sensitivity and fast response.

Keywords: Porous silicon; Zinc Sulfide; Heterojunction; Gas sensor
Received: 08 January 2024; **Revised:** 11 March 2024; **Accepted:** 18 March 2024

1. Introduction

Zinc sulfide (ZnS) is an inorganic semiconductor that has a wide direct bandgap (3.5-3.9eV). It possess a good thermal stability and high electronic mobility which is belonging to the halogen elements of the periodic table II-VI. The ZnS is attracted a lot of researchers, especially in the applications of ultraviolet light-emitting diodes (LEDs) [1], high carrier mobility, biosensors , solar cells and gas sensors [2]. The ZnS mixture shows two types of natural crystal shapes which are the cubic and the hexagonal shape. The cubic shape has a lattice constant of 0.541nm and is good match with Si. Therefore, an effective and homogeneous film of ZnS can be grown over the silicon substrate [3,4]. Moreover, an increase in the sensitivity of the gas sensor can be expected due to the increase in the absorbance of the molecules on the Porous Silicon (PSi) layer. Thus, PSi is used as bases instead of silicon wafers [5,6]. Several methods are used to synthesis the ZnS thin films such as, CVD, PECVD, sputter coater, sol-gel and spray pyrolysis [7]. Among of these methods, the spray pyrolysis method is easy to handle with, simple and inexpensive which is no need to complex devices. In addition, it is considered one of the most important methods for depositing a variety of materials in the form of a thin film [8]. Furthermore, high-quality thin film could be obtained using this method by controlling the temperature and the distance be-tween the substrate and the deposited materials. Also, the spray rate allows us to control the size of the droplets with homogeneously distribute along of heated substrate [9]. In addition, the PSi is attracted great attention due to its photoluminescence at room temperature in the visible light range [10]. Various techniques based chemical reaction are used to synthesis PSi over the surface of silicon (Si). The most widely used technique is the electrochemical etching method (ECE) because of its low cost and the possibility of obtaining high homogeneity and compatibility where alignment is required to initiate the chemical reaction [11]. The second method is photochemical reaction (PCE) via laser-induced etching which results in well-controlled light emission properties of the porous layer. The third method is photo-electrochemical etching (PECE), which is used to form and enhance the properties of the nanostructure layers for a wider PL range. The last method is spot etching of the silicon wafer in a solution based on HF:HNO_3:H_2O.The process of forming ZnS over PSi is carried out by spray pyrolysis method. This method is allow the form the particles size in nanoscale. Additionally, the concentration of the solution can be controlled easily to produce a final particle size that interested with. Using the spray pyrolysis, the process can be completed in short time just with a few seconds with high efficiency and homogeneous lattice compared to the other methods. [12,13]. The aim of this work is to fabricate the ZnS/PSi heterojunction as a sensor to detect NO_2 gas. The structural properties (XRD), surface properties (AFM and SEM), electrical for the fabricated sensor are studied.

2. Experimental Work

Porous silicon substrates were obtained by electrochemical etching of p-type (111) oriented silicon (c-Si) wafers with a resistivity of 1-10 Ω cm. Silicon wafers were cleaned with propanol and alcohol using an ultrasonic bath for 5 min. The c-Si wafers were rinsed with de-ionized water, dried with N2 flux, after that the samples immersed in mixed hydrofluoric acid (20%HF) and ethanol (99%). The anodizing cell consists of two cylinders made from Teflon with identical diameters. The upper layer contains a cylindrical cavity designated for the etching solution, while the lower layer is completely solid. The circle metal made from Stainless-steel is

placed on the lower cylinder and the Si wafer is placed on it and filled with an etching solution as shown in Figure 1a. The etching time was carried out for 5, 10, 15 min and the current density is fixed with 12 mA/cm^2 .

ZnS thin films over p-Si substrates was obtained by spray pyrolysis method. Zinc chloride ($ZnCl_2$) and sodium sulfide (Na_2S-Sigma Aldrich, reagent grade, 97% purity) were used as the source materials to produce the ZnS thin film. The $ZnCl_2$ and Na_2S were mixed in de-ionized water solutions at (0.1, 0.3 and 0.5M) as shown in table (1). The stirrer time of acetate solution was 40 min at room temperature. Next, the mixture was heated up to 85°C for one hour by magnetic stirrer. The final products were deposited over the glass substrates by chemical spray pyrolysis at 300°C and at the atmospheric pressure of 7.5 bar as shown in Fig. (1b). The reaction was investigated by the following equation [14]:

$$Na_2S(aq)+ZnCl_2(aq)\rightarrow ZnS(s)+2NaCl(aq) \quad (1)$$

Table (1) Preparation parameters of ZnS thin films

Concentration (mol)	0.1	0.3	0.5
Weight (gm) $ZnCl_2$	0.272	0.544	0.81789
Weight (gm) Na_2S	0.158	0.316	0.474

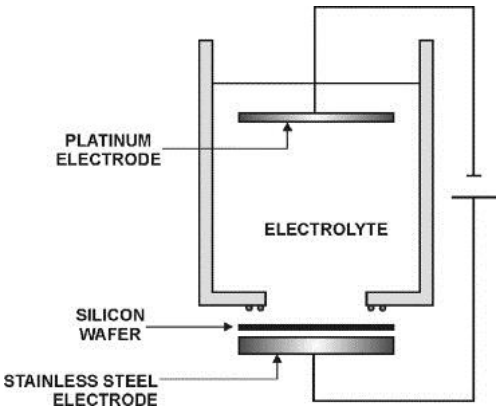

(a)

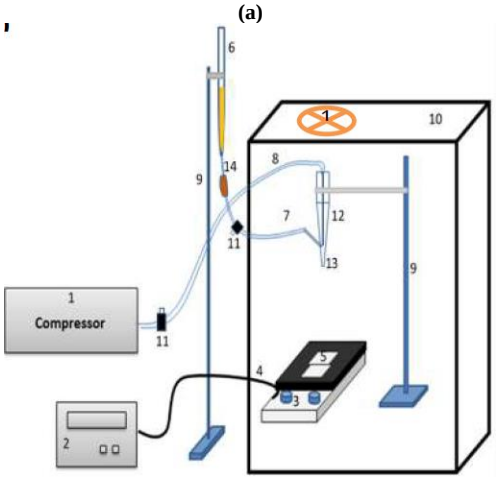

(b)

Fig. (1) (a) Electrochemical cell setup, and (b) spray pyrolysis setup

3. Results and discussion

The XRD patterns of the ZnS thin film deposited on glass substrates at concentrations of 0.1, 0.3 and 0.5M are shown in Fig. (2). It can be seen from this figure that all spectra show the peaks related to (111), (002), (110), (220) and (311) orientations corresponding to zinc-blende hexagonal structures according to JCPDS card No. 00–001–0677 wurtzite ZnS structure with an angle (2θ) equal to 31.13°, 27.32°, 38.06°, 48.31°, and 57.81°, respectively [15].

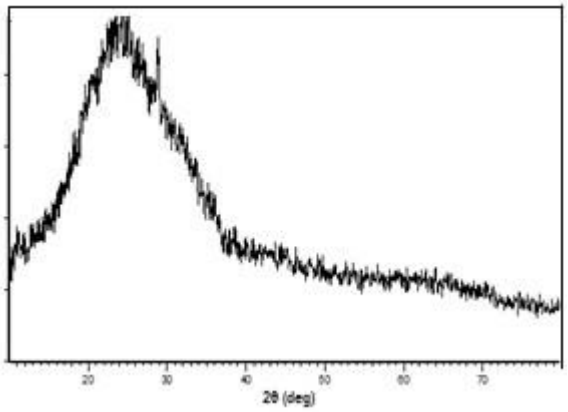

(a) 0.1 M

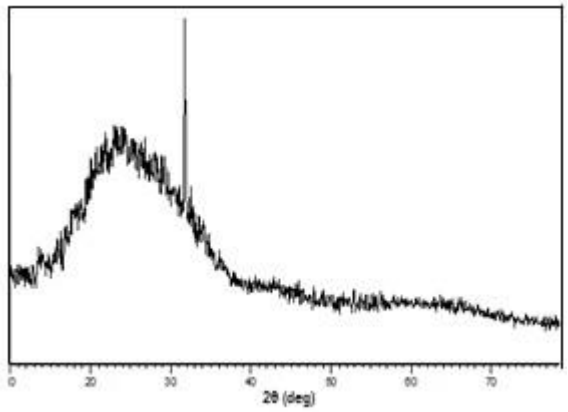

(b) 0.3 M

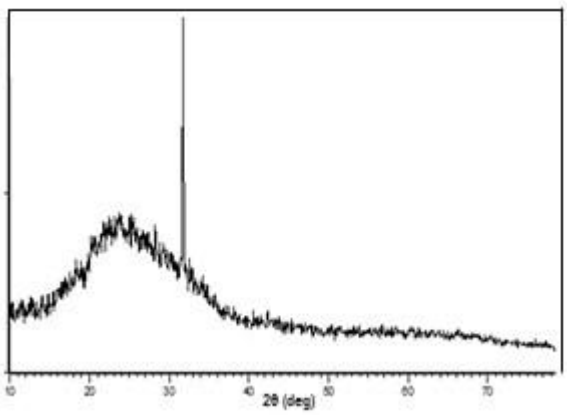

(c) 0.5 M

Fig. (2) XRD patterns of ZnS thin films deposited on glass substrate at concentrations of (a) 0.1M, (b) 0.3M and (c) 0.5M

Figure (3) shows the XRD pattern of ZnS/PSi heterojunction when the concentrations of ZnS are 0.1, 0.3 and 0.5M, respectively, at etching time of 10 min. It can be seen from Fig. (3a) that the PSi layer remains crystalline on planes of (111) and (002) with diffraction angle of 29.13° and 27.38°, respectively, which belong to wurtzite ZnS structure. Figure (3b) illustrates the peaks (002), (111) and (106) when the ZnS concentration of 0.3M which corresponding to diffraction angle 26.56°, 26.56° and 32.591°, respectively. Figure (3c) shows the diffraction angles of 30.06°, 27.27° and 38.06° belonging to (111), (002) and (110), respectively, when the ZnS concentration is 0.5M. It can be noted that the PSi peak is shifting slightly to small diffraction angle with increasing concentration. The FWHM of the peak is directly proportional to the crystallite size as shown in table (2).

The crystallite size (L) of PSi was calculated by Debye-Scherrer's formula [16,17]

$$L = \frac{k\lambda}{B\cos\theta} \qquad (2)$$

where λ is the x-ray wavelength, β is the full-width at half maximum (FWHM), and θ is the Bragg's angle

Figure (4) shows the surface morphology (2D and 3D) of porous silicon at different etching times (5 and 15 min). These images clearly show that the porous silicon with tightly branched pores has a sponge-like structure. Furthermore, the pore diameter and roughness of the surface increase with the increasing of etching time. This is attributed to extreme dissolution of PSi. Also, the porous silicon structure can be observed by uniform porosity structure with different pore diameters on the entire surface [18]. As a result, etching time may be employed to change the size and form the final pore structures. The average roughness of the pours is found to be 24.65 and 42.84 nm at etching time of 5 and 15 min, respectively. Figure (5) shows 2D and D AFM images of ZnS deposited on porous silicon substrates at concentration of 0.1M and different etching times (5 and 15 min). It is clear that the pore size expands when the ZnS heterojunction is synthesized [19]. Additionally, it can found that the PSi is completely covered by plentiful ZnS heterojunction. Subsequently, the surface distribution of the diameter values of the ZnS/PSi was randomly distributed and irregular heterojunction over the whole surface. The average roughness is found to be 83.36 and 93.32 nm at etching time of 5 and 15min, respectively. Table (3) indicates that the increasing in the etching time leads to increase the average diameter of the pores.

Figure (6) shows SEM images of ZnS deposited on glass substrates by spray pyrolysis method at concentrations of 0.1, 0.3 and 0.5 M. It indicates that the small regular grain size start to form on the glass substrate at ZnS concentration of 0.1M with circular grains as shown in Fig. (6a). When the ZnS concentration increases, the grain diameter also is increased as shown in figures (6b and 6c). The diameter of the ZnS nanoparticles it found to be 29, 37 and 58 nm at ZnS concentration of 0.1, 0.3 and 0.5 M, respectively.

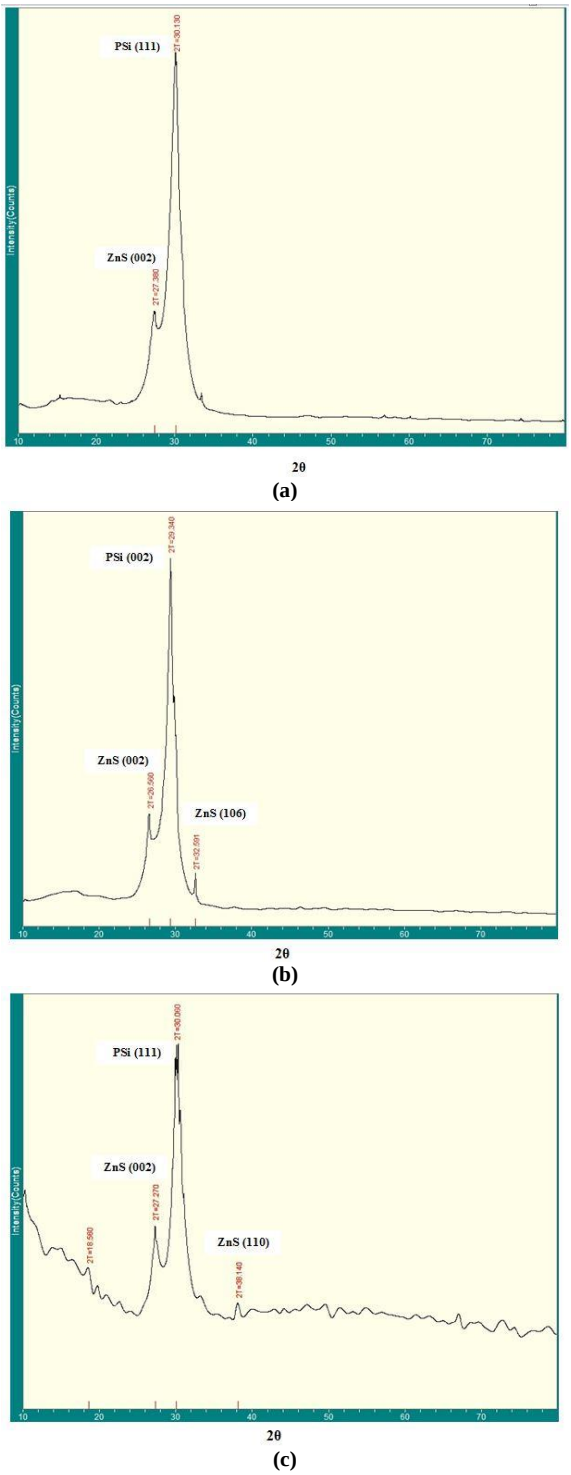

Fig. (3) XRD patterns of ZnS thin films deposited on porous silicon at concentrations of (a) 0.1M, (b) 0.3M and (c) 0.5M

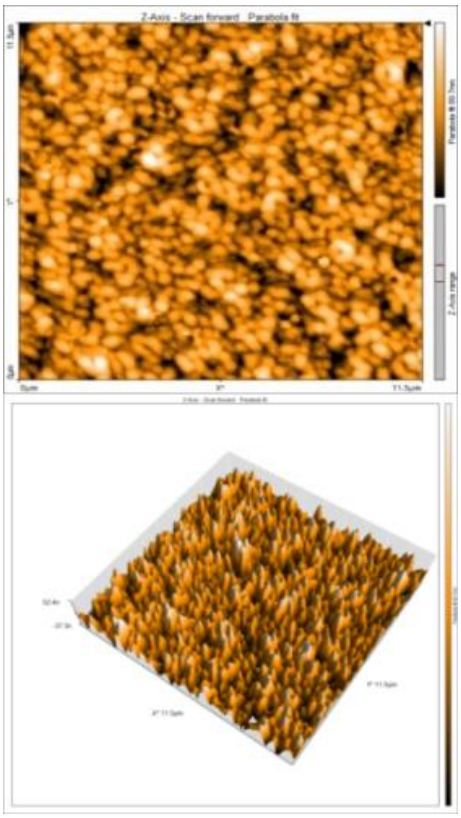

(a)

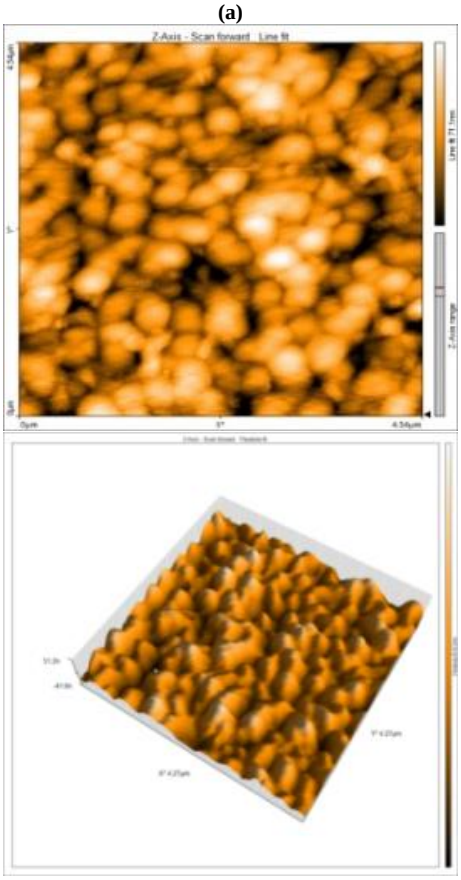

(b)

Fig. (4) AFM images for PSi at etching times of 5 and 15min

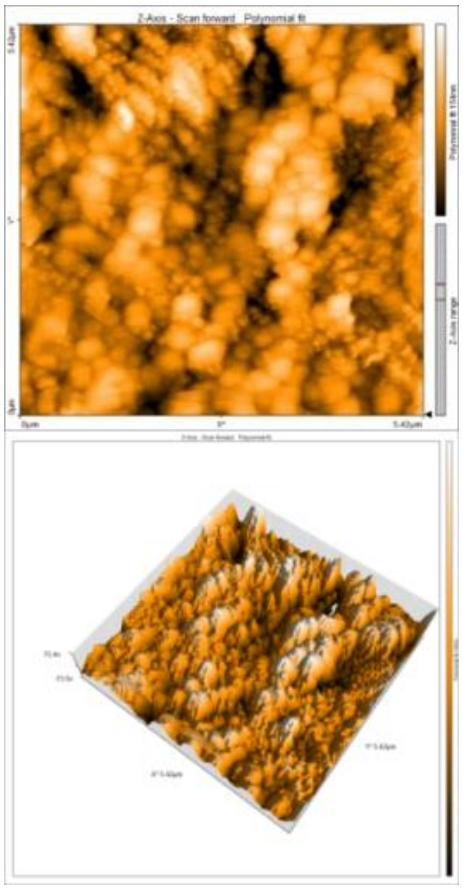

(a)

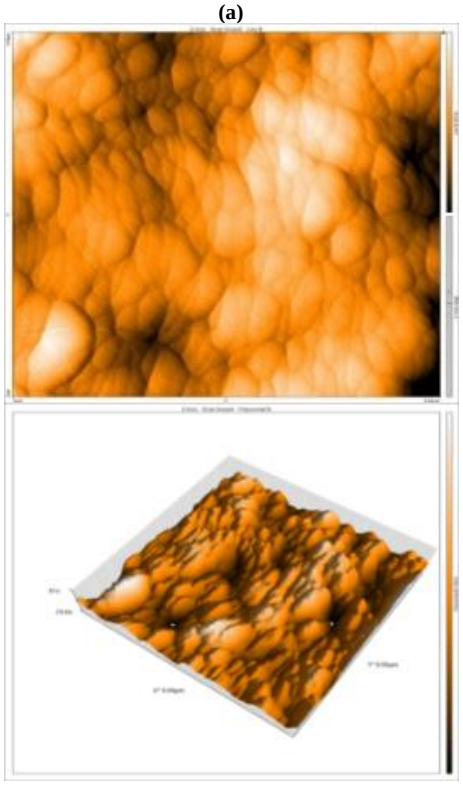

(b)

Fig. (5) AFM images of ZnS/Psi heterojunctions at etching times of 5 and 15 min when ZnS concentrations are 0.1 M and 0.5 M

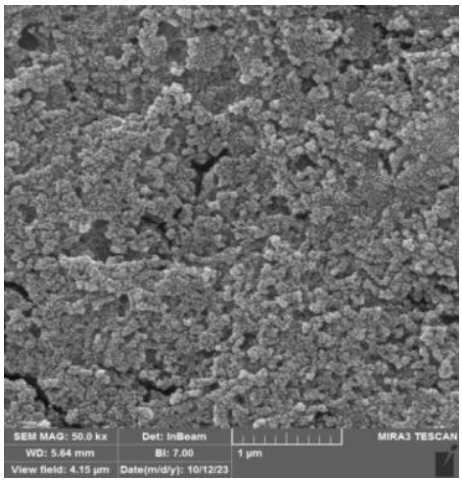

(a)

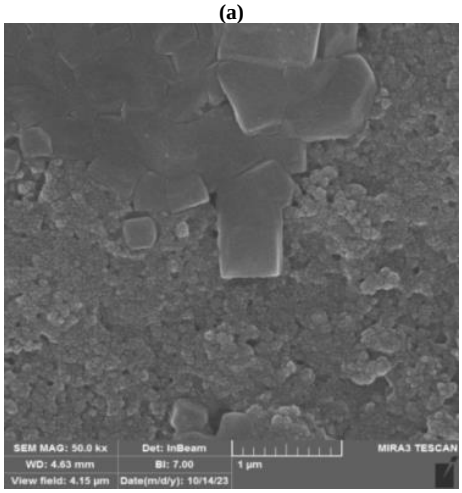

(b)

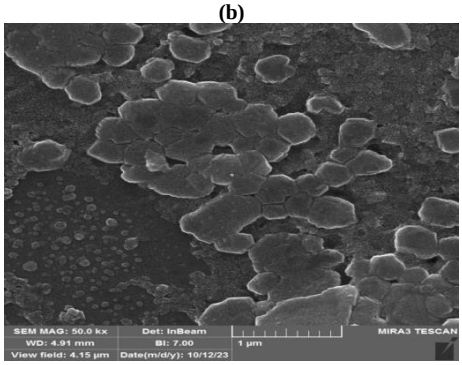

(c)

Fig. (6) SEM images of ZnS thin films on glass substrates at ZnS concentrations of (a) 0.1M, (b) 0.3M and (c) 0.5M

Figures (7a and b) show SEM images of PSi at etching time 5 and 15 min. The pore size increases with increasing the etching time due to dissolution of silicon substrate at the wall of pores. The images also approve star-like nanostructures with average diameter of 47nm. Figures (7c and d) show the SEM image of the ZnS/PSi surface at etching time 5 and 15 min respectively when the ZnS concentration is 0.3M.

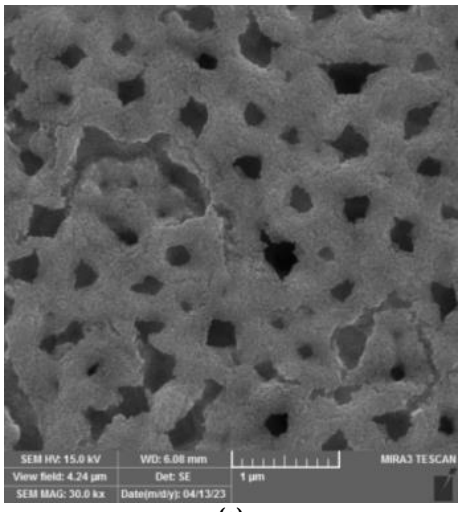

(a)

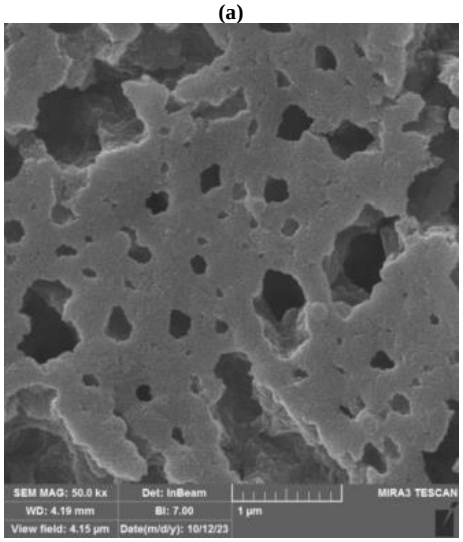

(b)

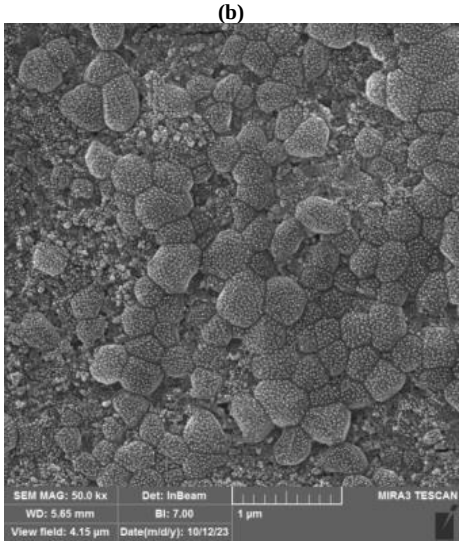

(c)

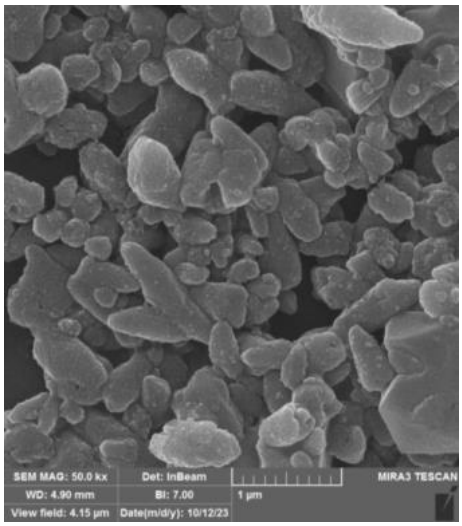

(d)

Fig. (7) SEM images (a) PSi at etching 5 min, (b) PSi at etching 15 min, (c) ZnS/PSi heterojunction of 0.3M at etching time 5 min and (d) ZnS /PSi of 0.3M at etching time 15 min

The results confirm that the agglomeration were observed with average diameter less than 100 nm [20]. Additionally, when the ZnS concentration increases, the nucleation stage of particle size is increased. We notice that there is a growth and interference between ZnS nanoparticls and the surface of the porous silicon, this interference increases with increasing etching time. The deposition of ZnS improves the structural stability of the porous silicon. Figure (8) shows the thickness of thin film as a function of the etching time. It can be notice that the thickness increases almost linearly when the etching time at all the ZnS concentration is increased. These results are agreement with previous works [21].

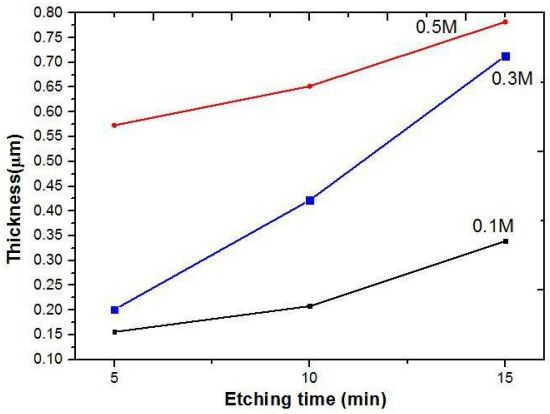

Fig. (8) Thickness of ZnS as a function of etching time with ZnS concentrations of 0.1M, 0.3M and 0.5M

Figure (9a) shows the EDS spectrum of ZnS deposited over the porous silicon at concentration of 0.1 M with etching time of 5 min. The strong spectrum shows the presence of Si, Zn and S at the appropriate energy levels. Furthermore, it is clear that the elements composition are found to be 44.10% Zn and 35.41% S at ZnS concentration of 0.5 M. In the other side, the elements mapping for Ca, Cl and Mg were presented due to aggregation and formation of ZnS nanostructure embedded porous silicon during preparation process [22] as shown in Fig. (9b). The values of all elements that appeared in the EDS spectra are shown in table (4).

Table (4) Elements values of EDS spectrum at ZnS concentration 0.1 and 0.5M with etching time 5 min

Element	0.1M	Line	0.5M
S	33.51	Ka	35.41
Ca	-	-	4.73
O	22.16	Ka	12.67
Cl	4.24	Ka	-
Mg	-	-	4.66
Zn	41.62	Ka	44.10
	100.00		100.00

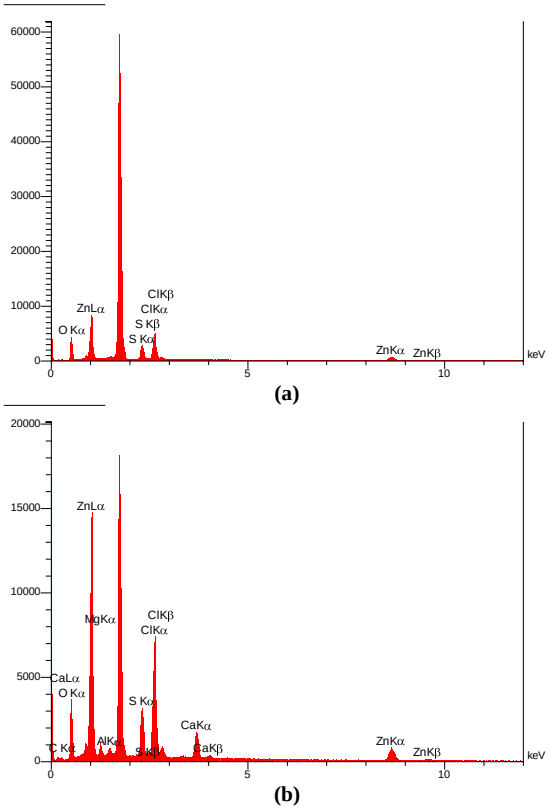

Fig. (9) EDS spectra of ZnS/PSi heterojunctions at ZnS concentrations of (a) 0.1M, and (b) 0.5M

The investigations of resistance, resistivity and conductivity were carried out for prepared gas sensor with ZnS concentrations of 0.1M and 0.5M that deposited over PSi at different etching times (5, 10 and 15 min). Figure (10) and figure (11) illustrate that the electrical conductivity increases with increasing the ZnS concentration for all samples. The obtained conductivity for the concentration of 0.5M is greater than the conductivity when the ZnS concentration is 0.1M. This is due to increase in the mobility of the charge carriers [23], and as a result, the ZnS thin films interference with the porous silicon and thus the conductivity increases. We also notice that the electrical conductivity increases with temperature.

This is attributed to improve the crystalline structure and caused a decrease in the grain boundaries due to increase in grain size [24].

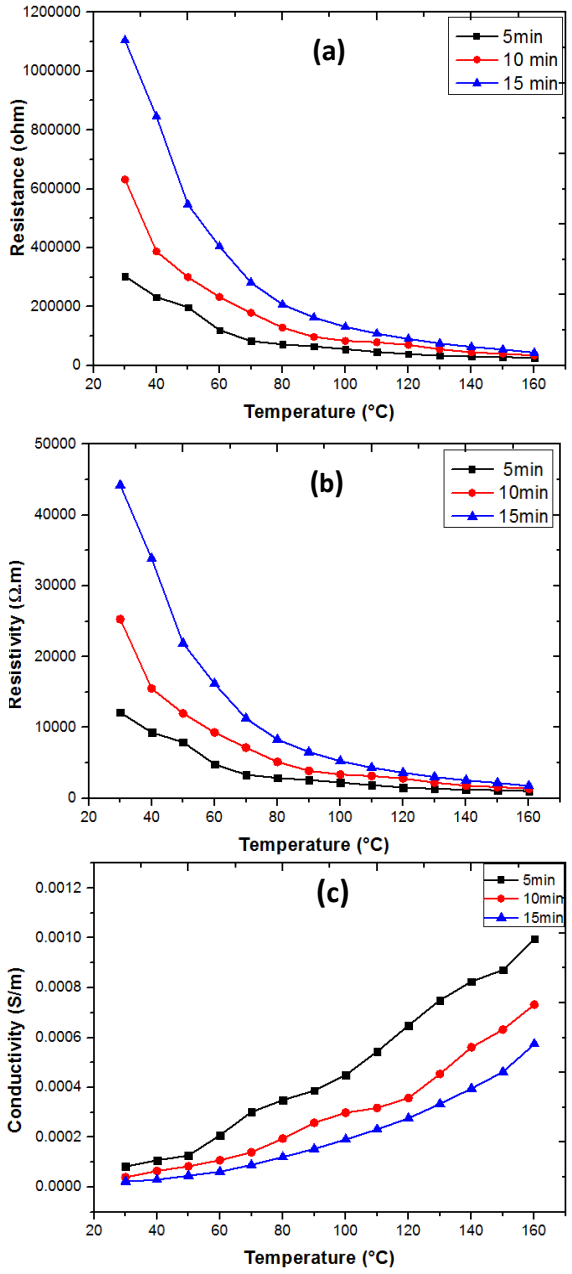

Fig. (10) Resistance, resistivity and conductivity of samples prepared at etching times of 5, 10 and 15min at concentration of 0.1M

Figure (12) shows the electrical characteristics (J-V) of ZnS/PSi heterojunction for forward and reverse bias. It can be notice that the samples have rectifier behave and the current density decreases with increasing etching time. As the dependence of the (J-V) characteristics on the etching time, is related to the formation of pores in porous silicon. When the pore diameter increases with increasing etching time, leads to an increase in resistivity of porous silicon due to the trapping of carriers at the walls of the pores. Furthermore, increasing in the etching time will also increase the thickness of the porous silicon thin film, and this leads to increase in resistivity due to a decrease in mobility with increasing etching time. We notice from these figures that there is increase in the current density with increase ZnS concentration, this is due to an increase in the carriers density that generated at the surface and the formation of additional levels, which in turn leads to an increase in electrical conductivity.

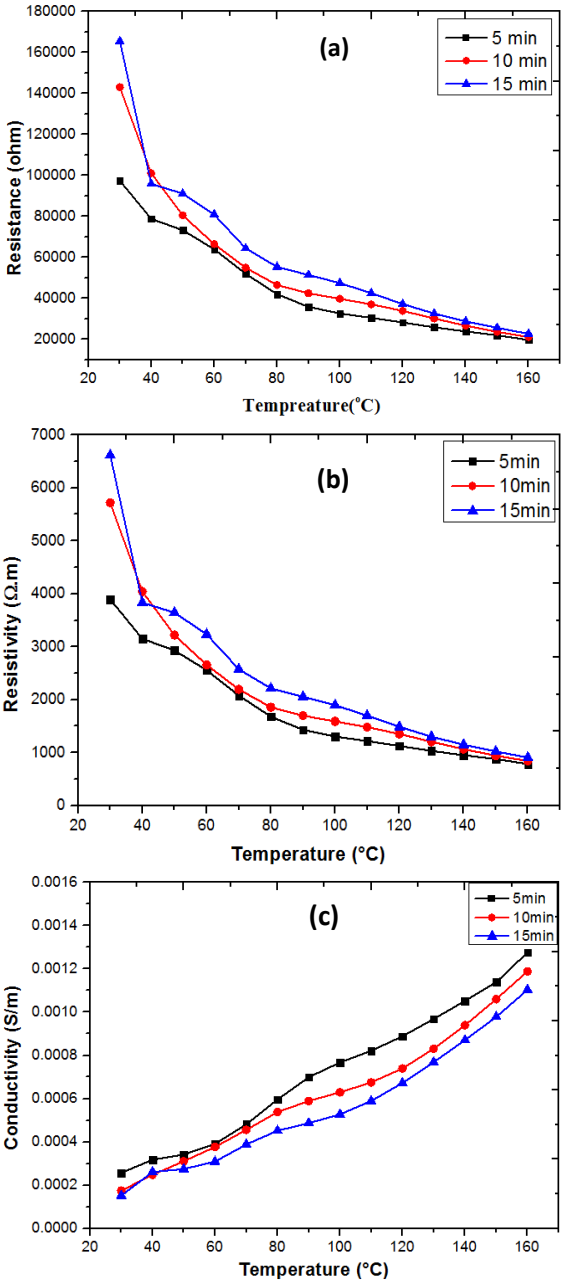

Fig. (11) Resistance, resistivity and conductivity of samples prepared at etching times of 5, 10 and 15min at concentration of 0.5M

The I-V characterization in forward bias possess two regions, the first region was found to be at low voltage ($1V < V_f$), where the current of this region is dominant because the concentration of carriers is greater than the pure state ($n_i^2 < np$). Therefore, in

order to reach a state of equilibrium, the recombination carriers process will be dominant, and this mean every electron is excited. At high voltages (V_f>1), the forward bias current increases exponentially with the applied voltages. In this case, the energy of carriers will increased with applied voltages and then it will pass through potential barrier of the ZnS-PSi heterojunction. Also, the ideality factor increases with increasing porosity due to an increase in the density of the levels at the interface between crystalline silicon and porous silicon. Table (5) shows the values of the reverse saturation cur-rent, ideality factor, barrier voltage and electrical conductivity for the ZnS/Psi heterojunction. Additionally, it can be seen that the values of the ideality factor and barrier voltage decrease with increasing concentration of ZnS [25].

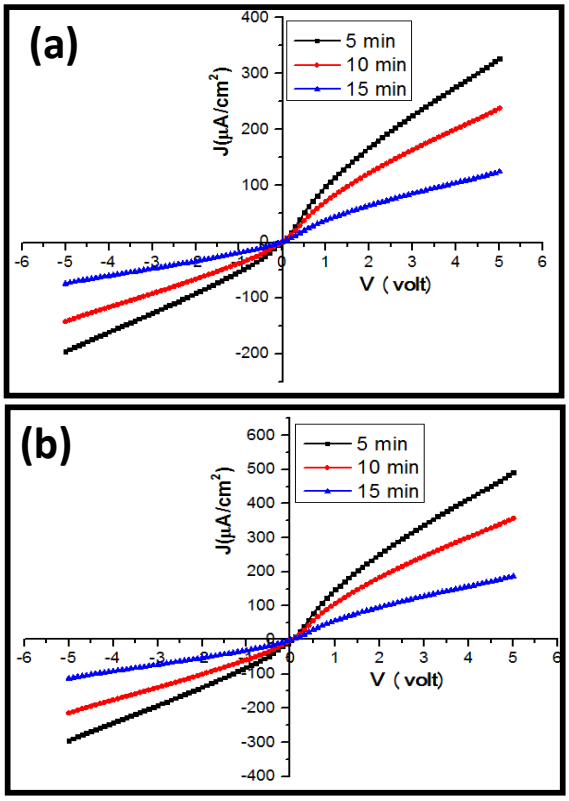

Fig. (12) J-V measurements of ZnS/PSi heterojunction with etching times of 5, 10 and 15 min at ZnS concentration (a) 0.1M and (b) 0.5M

Table (5) Parameters of Saturation current, ideality factor, barrier height and conductivity of ZnS/PSi heterojunction with etching time 5, 10 and 15 min at ZnS concentration 0.1 and 0.5 M

Etching time (min)	Concentration (M)	J_s (mA/cm²)	n	φ (eV)	σ ×10⁻³ (S/m)
5	0.1	12.27	2.43	0.635	0.997
10		6.92	2.68	0.669	0.732
15		1.64	2.79	0.72	0.575
5	0.5	17.86	2.31	0.613	1.28
10		11.21	2.48	0.632	1.19
15		6.56	2.63	0.690	1.10

Figures (13) and (14) (a-c) show the typical resistance response (kΩ) as a function to the time of gas sensor for different ZnS concentrations (0.1 M and 0.5 M). The operating temperature is selected as (RT, 100°C and 200°C) with constant NO_2 gas concentration of 75 ppm. The etching times of 5, 10 and 15 min are selected at ZnS concentration of 0.1 and 0.5M. The results illustrate that the significant variations of resistance for the gas sensor proved the synthesized ZnS over the porous silicon with higher purity and enabling their application in the manufacture of solid-state sensors for NO_2 detection. It is clear from these Figures that the resistance of ZnS/PSi heterojunction increased with increasing temperature. This can be attributed to increase the concentration which lead to increase the interactive between the surface area and the gas molecules [26]. The properties of ZnS/PSi heterojunction as a gas sensing for gases detection are examined. In order to determine the optimum operating temperature, the response of the ZnS /PSi heterojunction based gas sensors to 75 ppm of NO_2 is tested when the operating temperature varied from 50 to 250°C. Two concentrations of ZnS thin films of 0.1 M and 0.5 M are precipitated on the PSi. Figure (15) shows the sensitivity of sensor as a function of temperature for ZnS concentration of 0.1 and 0.5 M respectively when the etching time is varied from 5 to15 min with increment step of 5 min. It can be noted that the sensitivity of the sensor is varied with operating temperature. The sensitivity first is increased with increasing the temperature, up to 200°C, and then slowly decreased at 250°C. In addition, the sensitivity is improved for both concentration of ZnS when the time etching is increased. So, once size pore of PSi is changed, the sensitivity of ZnS /PSi heterojunction is change as well. Furthermore, the sensitivity is increased with increasing the ZnS concentration [27]. Figure (16) shows the comparison of the sensitivity for ZnS concentration of 0.1 and 0.5 M when the etching time is 15 min. As can be seen from this figure, the sensitivity of the ZnS/PSi heterojunction based gas sensor is increased with the increase the ZnS concentration. The maximum sensitivity is found to be 5.11 when the ZnS concentration is 0.5 M compared to the sensitivity of 3.0 at ZnS concentration of 0.1 M when the etching time of 15 min. This owing to increase the exposed surface area (increase the walls of the mesoporous structure), at this point, it is important to note that the Schottky barrier created at the ZnS/PSi interface due to the matching of the Fermi level, leading to create a depletion region and interactivity of surface area with gas molecules by the electron adsorption [28]. Tables (6-11) show response time, recovery time and sensitivity at different temperatures.

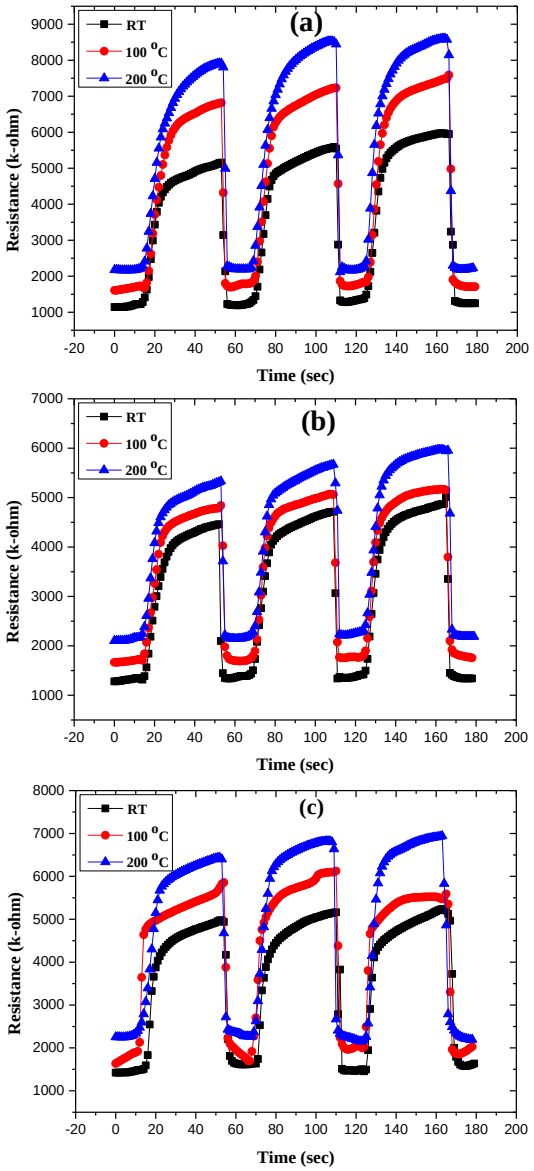

Fig. (13) Typical resistance curves of ZnS/PSi heterojunctions with ZnS concentration of 0.1M at different etching times (a) 5 min, (b) 10 min, (c) 15 min when the temperature is (RT, 100°C and 200°C) and 75 ppm of NO_2

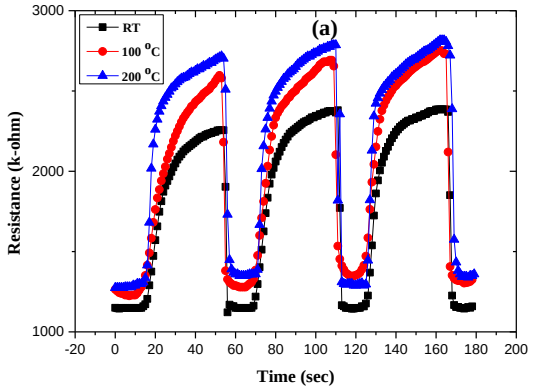

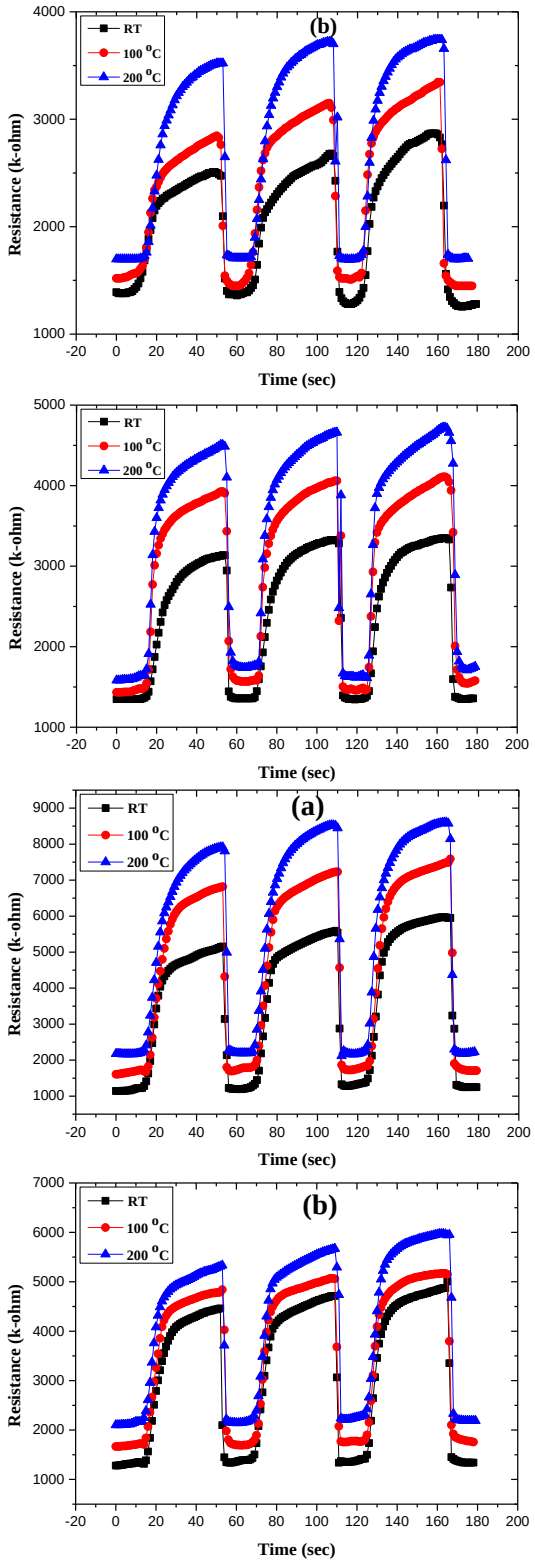

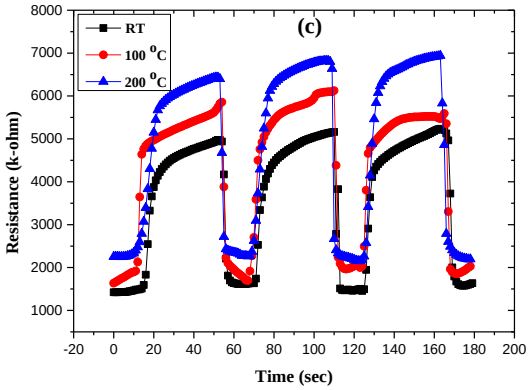

Fig. (14) Typical resistance curves of ZnS/PSi heterojunctions with ZnS concentration of 0.5M at different etching times (a) 5 min, (b) 10 min, (c) 15 min when the temperature is (RT, 100°C and 200°C) and 75 ppm of NO_2

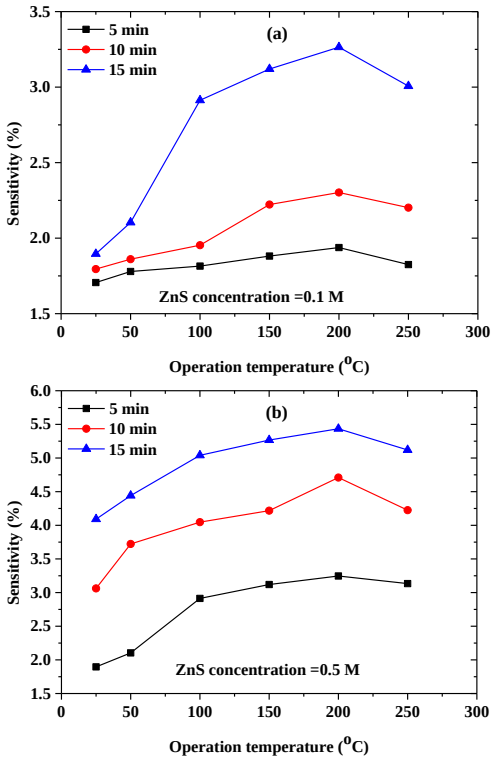

Fig. (15) Sensitivity versus operation temperature for NO_2 detection at etching times of 5, 10 and 15min and ZnS concentrations of (a) 0.1M, and (b) 0.5M

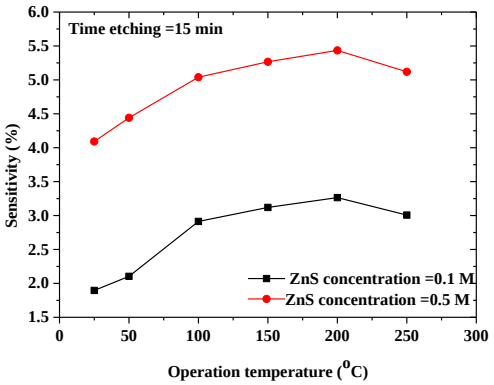

Fig. (16) The sensitivity comparison when ZnS concentrations are 0.1 and 0.5M at etching time of 15 min

4. Conclusions

In summary, good quality and high efficiency ZnS-PSi heterojunction-based gas sensors have been prepared by spray pyrolysis. The ZnS thin films are successfully grown on PSi substrates. The ZnS/PSi heterojunction-based gas sensors displayed good stability, fast response and recovery times and high sensitivity toward NO_2. The maximum sensitivity of the sensor is found to be 5.11 when the ZnS concentration is 0.5 M at operating temperatures up to 200°C. The results reveled that ZnS-PSi heterojunction is a promising candidate to use as photodetectors particularly for UV radiation.

Acknowledgements

The authors are thankful and gratitude to the Mosul University, College of Education for Pure Sciences, Department of Physics for providing all the required facilities.

References

[1] Sh.T. Hezarjaribi and N. Shahruz, "An enhanced fast ethanol sensor based on zinc oxide/nickel oxide nanocomposite in dynamic situations", *J. Inorg. Organometal. Polym. Mater.*, 30 (2020) 4072-4081.

[2] H.T. Hussein, U.M. Nayef and A.M. Hussien, "Synthesis of graphene on porous silicon for vapor organic sensor by using photoluminescence", *Optik*, 18(4) (2019) 61–70.

[3] Y.N. Al-Douri and C. Voon, "Etching time effect on optical properties of porous silicon for solar cells fabrication", *Optik*, 147(3) (2017) 343-349.

[4] O. Bisia, O. Stefano and L. Pavesi, "Porous silicon: a quantum sponge structure for silicon based optoelectronics Surface", *Sci. Rep.*, 38(12) (2000) 1-126.

[5] T. Kumeria, J.P. Steven and Sh.M. McInnes, "Porous silicon for drug delivery applications and theranostics: recent advances, critical review and perspectives", *Expert Opin. Drug Deliv.*, 14(12) (2017) 1407-1422.

[6] H. Föll et al., "New View of Silicon Electrochemistry", *phys. stat. sol. (a)*, 182(1) (2000) 7-16.

[7] A.A. Sulaiman, G.Gh. Ali and A.I. Thanon, "Synthesis and Study of ZnO Thin Films Using CVD Technique For Waveguide Sensor Applications", *J. Nanostruct.*, 12(1) (2022) 1-11.

[8] S. Mohammed, "Morphological and Optical Properties of Porous Silicon", *Eng. Technol. J.*, 37(1) (2019) 1-4.

[9] G.G. Ali, M.A. Ahmed and A.A. Sulaiman, "Structural properties of AuNPs/PSi nanostructure", *Digest J. Nanomater. Biostruct.*, 17(2) (2022) 473-480.

[10] J. Park, Y. Yanagida and T. Hatsuzawa, "Fabrication of p-type porous silicon using double tank electrochemical cell with halogen and LED light sources", *Sen. Actuat. B: Chem.*, 233(11) (2016) 136-143.

[11] E.A. Saverina, "Porous Silicon Preparation by Electrochemical Etching in Ionic Liquids", *ACS Sustain. Chem. Eng.*, 8(27) (2020) 10259-10264.
[12] J. Andrew and R. James, "Pyrite Formation via Kinetic Intermediates through Low-Temperature Solid-State Metathesis", *J. Am. Chem. Soci.*, 136(44) (2014) 15654-15659.
[13] C. Wang, "Structure and photoluminescence properties of ZnS films grown on porous Si substrates", *Opt. Laser Technol.*, 43(8) (2011) 1453-1457.
[14] I. Syahidi, B. Prayogo and K. Triyan, "Porous silicon fabrication on n-type Si (111) electrochemical anodization technique with HF: methanol solution", *Mater. Today: Proc.*, 44(7) (2021) 3430-3433.
[15] U.M. Nayef, H.T. Hussein and A.M. Abdul Hussien, "Study of photoluminescence quenching in porous silicon layers that using for chemical solvents vapor sensor", *Optik*, 172(7) (2018) 1134-1139.
[16] H.P Wang et al., "Fabrication of silicon hierarchical structures for solar cell applications", *IEEE Access*, 7(2) (2018) 19395-19400.
[17] J. Xu, "Preparation of porous silicon by electrochemical etching methods and its morphological and optical properties", *Int. J. Electrochem. Sci.*, 14(2) (2019) 5188-5199.
[18] X. Yang et al., "Porous Silicon Fabrication and Surface Cracking Behavior Research Based on Anodic Electrochemical Etching", *Fuel Cells*, 21(1) (2020) 52-57.
[19] K. Omar and K.A. Salman, "Effects of electrochemical etching time on the performance of porous silicon solar cells on crystalline n-type (100) and (111)", *J. Nano Res.*, 12(2) (2017) 123-134.
[20] R. Vercauteren, "Porous silicon membranes and their applications: Recent advances", *Sens. Actuat. A: Phys.*, 318(12) (2020) 112486.
[21] O.S. Volovlikova and P. Lazarenko, "Influence of illumination on porous silicon formed by photo-assisted etching of p-type Si with a different doping level", *Micromachines*, 11(2) (2020) 199.
[22] M.S. Akhtar, "Surfactant and template free synthesis of porous ZnS nanoparticles", *Mater. Chem. Phys.*, 189(3) (2016) 28-34.
[23] Y. Tsai, "Morphological and crystalline analysis of ZnO/ZnS nanostructures on porous silicon substrate", *Vacuum*, 178(8) (2020) 109454.
[24] D.A. Lizunkova, I.A. Shishkin and N.V. Latukhina, "Optical and photoelectric characteristics of the ZnS/porous-Si/Si structure performed by different technological routes", *IOP Publish.: Conf. Ser.*, 1 (2020) 1695.
[25] M. Mizuhata, M. Yuki and M. Hideshi, "Fabrication of ZnS/Porous silicon composite and its enhancement of photoluminescence", *Electrochimica Acta*, 201(3) (2016) 86-95.
[26] I. Sadovnikov, "Synthesis, properties and applications of semiconductor nanostructured zinc sulfide", *Russian Chem. Rev.*, 88(6) (2019) 571-582.
[27] A. Kumar, "Highly responsive and low-cost ultraviolet sensor based on ZnS/p-Si heterojunction grown by chemical bath deposition", *Sens. Actuat. A: Phys.*, 331(5) (2021) 112988.
[28] M.M. Hassan and M.A. Fakhri, "2-D of Nano Photonic Silicon Fabrication for Sensing Application", *Digest J. Nanomater. Biostruct.*, 14(4) (2019) 873-878.

Table 2: crystalline size , FWHM, inter-plane distance (d) of ZnS/PSi

Sample	Concentration (M)	2θ	hkl	L (nm)	FWHM (deg)	d (Å)
ZnS/PSi	0.1	27.38	002	37.47	0.561	3.254
		29.13	111	29.561	0.826	3.431
ZnS/PSi	0.3	26.56	002	38.615	0.436	3.174
		29.34	111	30.422	0.723	3.255
		32.591	106	22.633	0.985	3.513
ZnS/PSi	0.5	27.27	002	39.711	0.411	3.251
		29.06	111	33.622	0.633	3.122
		38.06	110	24.799	0.911	3.422

Table 3. The optimization parameters of ZnS/PSi heterojunction as a gas sensor

Sample	Concentration of ZnS (M)	Roughness Average (nm)	RMS (nm)	Diameter Average (nm)
PSi	-	1.26	1.31	24.65
	-	2.06	2.11	42.84
ZnS/PSi	0.3	2.53	1.88	83.36
	0.3	2.67	1.96	93.32

Table (6) Parameters of gas sensor for detect NO_2 gas of 75 ppm at different temperature, etching time of 5 min and ZnS concentrations of 0.1M

	RT	50°C	100°C	150°C	200°C	250°C
Air	1121.66	1224.047	1231.422	1231.422	1271.422	1251.422
Gas	3035.241	3.40E+03	3.47E+03	3548.241	3735.241	3535.241
G% (NO_2)	1.706026	1.779078	1.814822	1.881418	1.937846	1.82498
Response time (s)	4.3	5.8	8.2	11.8	13.51	15.62
Recovery time (s)	3.6	3.1	2.9	2.3	2.1	1.9

Table (7) Parameters of gas sensor for detect NO_2 gas of 75 ppm at different temperature, etching time of 10 min and ZnS concentrations of 0.1M

	RT	50°C	100°C	150°C	200°C	250°C
Air	1121.66	1224.047	1241.422	2154.084	1854.848	1322.426
Gas	3135.241	3501.723	3666.233	6941.776	6125.057	4234.195
G% (NO_2)	1.795179	1.860774	1.953254	2.222612	2.302188	2.20184
Response time (s)	8.2	9.2	6.5	8.9	9.4	10.2
Recovery time (s)	2.1	2.3	2.3	2.4	2.7	2.5

Table (8) Parameters of gas sensor for detect NO_2 gas of 75 ppm at different temperature, etching time of 15 min and ZnS concentrations of 0.1M

	RT	50°C	100°C	150°C	200°C	250°C
Air	1232.676	1665.708	1280.158	1240.158	1260.158	1250.158
Gas	3569.528	5170.168	5009.304	5109.304	5209.304	5009.304
G% (NO_2)	1.895755	2.103886	2.913035	3.11988	3.133849	3.006936
Response time (s)	4.2	5.3	4.9	6.8	6.9	7.5
Recovery time (s)	2.4	2.3	2.1	1.9	1.8	1.7

Table (9) Parameters of gas sensor for detect NO_2 gas of 75 ppm at different temperature, etching time of 5 min and ZnS concentrations of 0.5M

	RT	50°C	100°C	150°C	200°C	250°C
Air	1232.676	1665.708	1280.158	1240.158	1250.158	1260.158
Gas	3569.528	5170.168	5009.304	5109.304	5309.304	5209.304
G% (NO_2)	1.895755	2.103886	2.913035	3.11988	3.246905	3.133849
Response time (s)	6.3	7.8	11.3	13.2	15.4	17.2
Recovery time (s)	3.1	2.8	2.3	2.1	1.9	1.8

Table (10) Parameters of gas sensor for detect NO_2 gas of 75 ppm at different temperature, etching time of 10 min and ZnS concentrations of 0.5M

	RT	50°C	100°C	150°C	200°C	250°C
Air	2118.303	1606.957	1250.158	1144.121	1280.158	1380.158
Gas	8604.078	7588.949	6309.304	5969.713	7309.304	7211.304
G% (NO_2)	3.061779	3.722559	4.046804	4.21773	4.709687	4.224983
Response time (s)	6.3	7.4	11.5	12.5	13.7	15.2
Recovery time (s)	2.8	2.4	2.1	2.2	2.1	1.9

Table (11) Parameters of gas sensor for detect NO_2 gas of 75 ppm at different temperature, etching time of 15 min and ZnS concentrations of 0.5M

	RT	50°C	100°C	150°C	200°C	250°C
Air	1239.158	1244.121	1210.158	1230.158	1260.158	1231.422
Gas	6309.304	6769.713	7309.304	7709.304	8109.304	7535.241
G% (NO_2)	4.091604	4.441363	5.039957	5.26692	5.435147	5.119139
Response time (s)	7.8	8.1	8.3	8.6	9.3	9.7
Recovery time (s)	2.6	2.3	1.9	1.7	1.6	1.5

